Dentomaxillofacial Radiology (2014) 43, 20130237

http://dmfr.birjournals.org

RESEARCH

Diagnostic value of CT perfusion imaging for parotid neoplasms

Y Dong, G-w Lei, S-w Wang, S-w Zheng, Y Ge and F-c Wei

Department of Radiology, the First Affiliated Hospital of Dalian Medical University, Dalian, China

Objectives: To assess the value of CT perfusion imaging in the differentiation of different histological categorization of benign tumours from malignant tumours in patients with parotid neoplasms.
Methods: CT perfusion was successfully performed in 62 patients with parotid neoplasms whose diagnoses were confirmed by surgery or biopsy. The software generated a tissue time–density curve (TDC) and measured blood volume, blood flow, mean transit time and capillary permeability surface product. One-way ANOVA and receiver operating characteristic curves were used to analyse the difference and diagnostic efficacies of all perfusion data between each one of the benign tumours and malignancies. Statistical significance was assigned at the 5% level.
Results: Pleomorphic adenomas mainly had a gradually ascending TDC. Warthin tumours showed a fast ascent followed by a fast descent. The TDC of basal cell adenomas had a fast ascension followed by a plateau, then a gradual descent. Malignant tumours mainly showed a rapidly ascending curve with a stable plateau. Significant differences were observed in blood flow, blood volume and mean transit time between pleomorphic adenomas and malignant tumours ($p < 0.05$) as well as in blood flow and blood volume between the Warthin tumours, the basal cell adenomas and the malignant tumours ($p < 0.05$). Differences in permeability surface between the basal cell adenomas and malignant tumours were significant ($p < 0.01$).
Conclusion: CT perfusion of parotid gland could provide TDC and perfusion data, which were useful in the differentiation of different histological benign tumours and malignant tumours in the parotid gland.
Dentomaxillofacial Radiology (2014) **43,** 20130237. doi: 10.1259/dmfr.20130237

Cite this article as: Dong Y, Lei G-w, Wang S-w, Zheng S-w, Ge Y, Wei F-c. Diagnostic value of CT perfusion imaging for parotid neoplasms. *Dentomaxillofac Radiol* 2014; **43:** 20130237.

Keywords: parotid gland; neoplasms; computed tomography; perfusion

Introduction

The parotid glands are the largest paired aggregates of salivary tissue in the body. The acinar, ductal and myoepithelial cells that comprise parotid tissue can give rise to an almost bewildering variety of benign and malignant neoplasms.[1,2] These neoplasms have similar clinical symptoms and image features. From the clinical aspect, malignant tumours are painless palpable masses and cannot be differentiated from benign tumours.[3] The diagnostic process of salivary gland tumours is challenging. With view to the patient's prognosis and the required treatment, pre-operative knowledge of the tumour type would be of outstanding importance, as malignancies require radical tumour resection with lymph node dissection and adjuvant radio- (chemo) therapy.[3] Fine-needle aspiration cytology is helpful in differentiating a neoplasm from a non-neoplastic lesion, although it has a high specificity but a lower sensitivity for neoplastic parotid lesions. In a current meta-analysis by Schmidt et al,[4] the actual sensitivity and specificity after bias correction for diagnosis of a neoplasia are estimated to be 71% and 100%, respectively. It is possible that pre-operative imaging is a more appropriate approach to the workup of these tumours.

Multislice CT is the primary imaging modality for parotid gland pathologies. Dual-phase enhanced examination has excellent spatial and temporal resolution and has been currently the main imaging technique for the

Correspondence to: Dr Yue Dong. E-mail: dyy1026@sina.com
Supported by the science and technology fund of the Dalian Science and Technology Bureau. Project ID: 2010J21DW023.
Received 5 July 2013; revised 21 October 2013; accepted 29 October 2013

assessment of parotid gland lesions.[2,5] A study found that the percentage washout ratios in contrast material-enhanced CT may reflect various characters of parotid gland neoplasms and assist in differentiating benign from malignant tumours.[6] However, conventional CT enhanced scanning can only provide two or three phases enhanced pattern of the lesions, and it does not provide absolute quantification of perfusion changes in parotid gland lesions. CT perfusion (CTP) imaging involves the non-invasive measurement of blood volume of the lesions at the capillary level. Compared with dual-phase enhanced scanning, CTP can provide time–density curves (TDCs) that show the dynamic change of blood supply at multiple time points. CTP has been used for differentiation between benign and malignant masses in various organs.[7–10] CTP is now recognized as an important method that can provide valuable information in patients with head and neck masses.[7,11–14]

The purpose of this study is to investigate the TDC types and perfusion parameters in the diagnosis and differentiation of parotid lesions.

Methods and materials

Patients

The approval from the Human Subjects Committee at our institution was obtained prior to performing this prospective study, and informed consent was obtained from all patients prior to enrolment in this study. 64 patients received CTP of the parotid gland for a single mass of the parotid gland; of these, 2 cases were excluded because of CTP failure, whereas 62 cases were included in this research (30 males and 32 females; mean age, 53.1 ± 16.6 year; range, 20–82 years). In all patients, surgery or biopsy was performed after the CT examination; 58 cases had parotidectomy, and 4 cases had biopsy performed.

CT imaging protocol

All patients were examined using 16-detector multislice CT scanner (LightSpeed™ Ultra; GE Medical Systems, Milwaukee, WI). A non-enhanced CT examination (120 kV and 80 mA with a pitch of 1 and 2.5 mm contiguous sections and 1 s scan time) was performed initially from the skull base to the thoracic inlet, followed by reconstruction using the soft-tissue algorithm. A supervising radiologist with 10 years' experience selected a perfusion CT volume, which was centred on the parotid tumour at its widest dimension on the CT axial images. For CTP, 50 ml of a non-ionic contrast agent (370 mg of iodine per millilitre; Ultrovist™; Schering, Berlin, Germany) was injected at a rate of 4 ml s^{-1} using a power injector. At 5 s after the initiation of the injection, a cine continuous scan was initiated with the following technique: 200 mA, 80 kVp, 4 × 5 mm sections, 1 s per rotation for the duration of 45 s. The contrast agent administration was followed by a power injection of 20 ml of saline (at the same injection rate). The total radiation dose received by each patient during the whole procedure was 267 mGy, which is within the annual permitted limit. Before the perfusion scan, the patients were asked to take off the false teeth and not to swallow to limit laryngeal motion.

Post-processing of the perfusion data and image analysis

All PCT images were analysed at separate workstations by using commercial deconvolution-based perfusion CT software (Perfusion™ 3.0; GE Healthcare, Milwaukee, WI) and the body tumour perfusion algorithm. A representative 5 mm tumour section was selected. A single observer (a radiologist with 3 years' experience), aware of the primary tumour site, generally placed a region of interest on the ipsilateral external carotid artery and external jugular vein. The ipsilateral internal carotid artery was chosen as the artery input in those patients whose external carotid artery was not reliably identified in cross section. With a processing threshold ranging from −30 to 400 HU, colour coded maps of blood flow (BF), blood volume (BV), mean translate time (MTT) and capillary permeability surface (PS) were generated. A free-hand region of interest was then drawn around the primary tumour periphery, excluding the large feeding vessels, gross cystic, necrotic or hemorrhaged areas and the surrounding visually not infiltrated tissue. The software then generated a tissue TDC and four perfusion parametric values (BF, BV, MTT and PS) for the selected ROIs. The BF, BV, MTT and PS values from the tumour site were calculated by averaging the perfusion values for the best three of four sections to get perfusion values as accurate as possible.

Statistical analyses

All statistical analyses were performed using statistical software, SPSS® v. 17.5 (SPSS Inc., Chicago, IL). The mean values (with standard deviations) of all perfusion parameters were calculated. One-way ANOVA was used to analyse statistical difference of all perfusion parameters between each one of the benign tumours and malignancies in the parotid gland. Statistical significance was assigned at the 5% level. Receiver operating characteristic (ROC) curves were used to estimate the diagnostic efficacies of perfusion data in the identification of each one of the benign tumours and malignancies. The area under ROC curve (ROC area) was calculated for each variable. The optimal threshold for a variable was determined from its ROC analysis by evaluating the sensitivity and specificity.

Results

Of the 64 trials, artefact from laryngeal motion affected CT perfusion analysis in 2 cases, so these 2 were excluded and the remaining 62 cases were included in this research. Histopathology showed that the 62 cases included 20 pleomorphic adenomas, 19 Warthin tumours, 6 basal cell tumours and 17 malignant lesions (5 metastases, 4 squamous cell carcinomas, 2 mucoepidermoid carcinomas, 1

malignant pleomorphic adenoma, 1 duct cell carcinoma, 1 basal cell carcinoma, 1 acinic cell carcinoma, 1 lymphoma and 1 adenocarcinoma).

The obtained TDCs were classified into four types (Figure 1) on the basis of the time to peak (TTP) and the washout ratio (WR). These TDC parameters were calculated using the following equations: TTP = time required to reach the enhancement density peak; WR (%) = {[(density at peak) − (density at 50 s after the start of contrast medium injection)] × 100}/[(density at peak) − (density at the start of contrast medium injection)]. TDC patterns (A–D) are as follows (Figure 1). Type A TDCs were those with TTP above 30 s and no washout, Type B TDCs had TTP less or equal to 30 s and WR >30%. Type C TDCs were those having TTP less or equal 30 s and with WR ranging from 10% to 30%. Type D TDCs had a TTP of 30 s or less with a WR <10%.

Table 1 summarises the results for the TDC patterns of different pathological entities in parotid gland. There was minor overlapping of the different types of perfusion curves. The majority of pleomorphic adenomas and a few malignant lesions had Type A TDC. Type B characterized Warthin tumours. Type C represented mostly basal cell adenomas but included some malignant

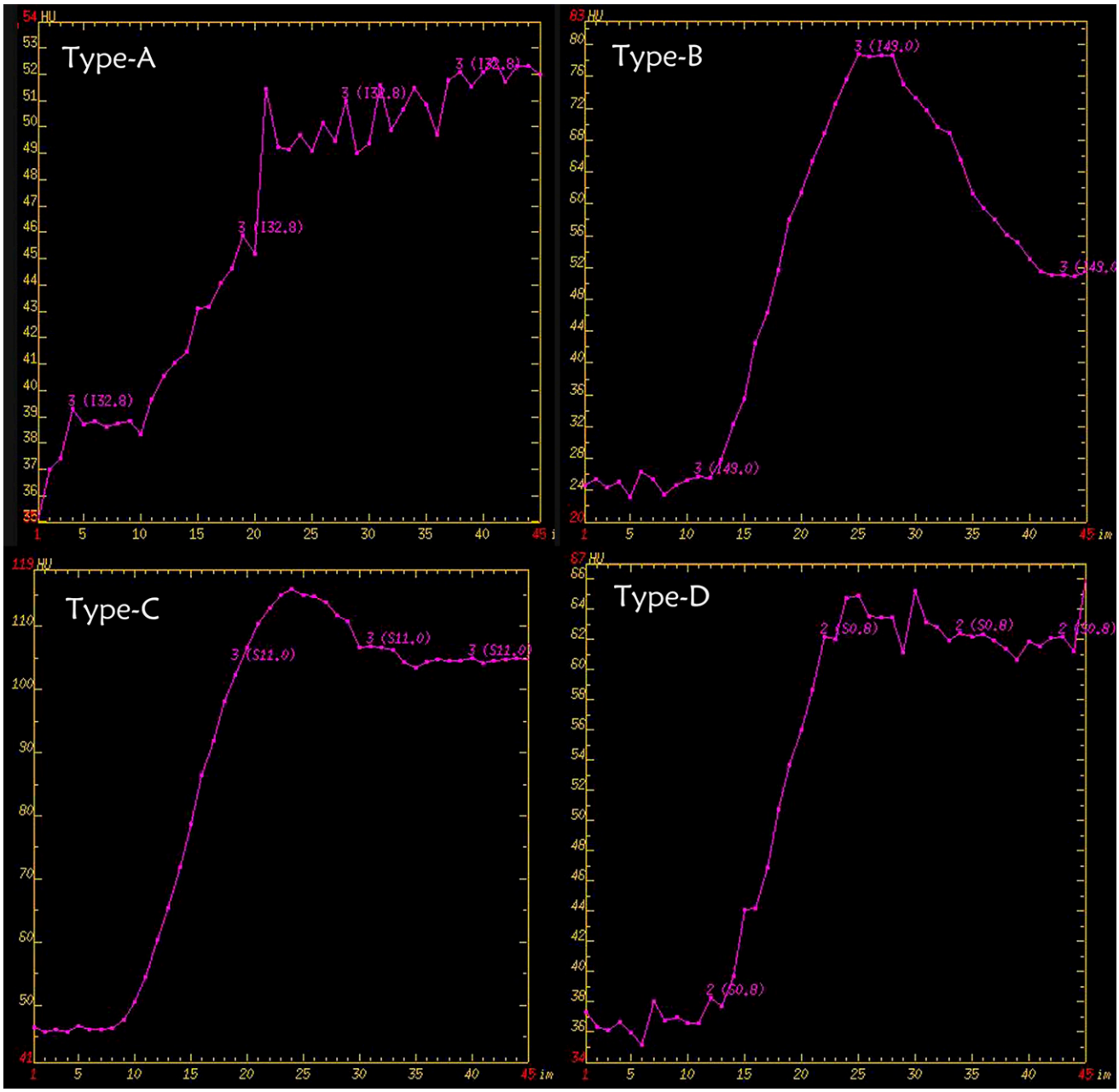

Figure 1 The four different types of time–density curves.

Table 1 TDC patterns for different pathological entities of the parotid gland

	Time–density curve types			
Pathological entities	*A*	*B*	*C*	*D*
Pleomorphic adenomas	17	–	–	3
Warthin tumours	0	19	–	–
Basal cell adenomas	–	–	6	–
Malignant lesions	3	0	4	10

tumours. Although three pleomorphic adenomas showed Type D, it was mostly a characteristic of the malignant tumour group.

Table 2 summarises the results for BF, BV, MTT and PS in different pathologies. Statistical analysis showed a significant difference between the pleomorphic adenomas and the malignant tumours in BF, BV and PS ($p < 0.05$), with the pleomorphic adenomas having relatively lower BF, BV and PS. Statistically significant differences were also observed between the Warthin tumours, basal cell adenomas and the malignant tumours in BF and BV ($p < 0.05$), with the Warthin tumours and the basal cell adenomas having relatively higher BF and BV. Differences in PS between the basal cell adenomas and the malignant tumours were significant ($p < 0.01$), with the basal cell adenomas having higher PS (Figures 2–5).

Tables 3–5 show the ROC area, thresholds and diagnostic efficacy of perfusion data for distinguishing different benign tumours from malignant tumours. The BF and BV have higher diagnostic efficacies than MTT and PS for the differentiation of pleomorphic adenomas, Warthin tumours and malignant tumours. The BF, BV and PS have higher diagnostic efficacies than MTT for the differentiation of basal cell adenomas and malignant tumours.

Discussion

Perfusion can be defined as the blood flow through a tissue of interest per unit of volume. After an intravenous bolus injection of an iodinated contrast agent, attenuation changes in vessels and tissue can be observed during the first pass by means of dynamic image acquisition at a given anatomical level. TDC can then be constructed for reader-defined ROIs.[7,15,16] The time course of the iodine concentration is a measure of the regional perfusion, and this concentration is linearly correlated to tissue attenuation values, as seen on CT. The deconvolution-based calculation of these parameters is the method we used. Deconvolution of arterial and tissue enhancement curves is a complex mathematical process that gives the blood flow as the height of the plateau, whereas blood volume is calculated as the area under the curve. The equation MTT = blood volume/blood flow can then be used to obtain the MTT.[7,15,16] Permeability surface represents the transmission rate of contrast media from capillary endothelium to interstitial space and reflects the integrity of endothelial cells and permeability of vessels. It is known that tumour capillaries, in general, have wide interendothelial junctions, a large number of fenestrate and transendocannels and discontinuous or absent basement membrane, which are spectrally common in malignant tumours.[15,16]

In this study, the rate of performing a successful CTP was 96.8%. Thus, CTP is feasible in the parotid gland. Only two patients could not control their laryngeal motion. As a result, there were movement artefacts on the CTP primary images. Consequently, TDCs and perfusion data maps were flawed, that is why the two cases were not included in the research. Compared with chest and abdomen, head and neck tissue is stable and generally without movement artefact. So, CTP was not affected by breathing.[7–9] It is only when the position of the lesion is at the level of the larynx that the laryngeal motion would affect the achievement of satisfactory TDCs. In fact, a previous study mentioned that laryngeal motion was an important reason for unsuccessful CTP.[7] Nevertheless, the false teeth also could cause some artefacts and make the TDC unsuccessful. So, before the perfusion scanning, it is necessary to take off the false teeth and ask the patient not to swallow to limit laryngeal motion. In contrast to previous studies of head and neck tumours using CTP,[7,11–14] this study focused on the evaluation of the TDC patterns and perfusion parameters in different parotid pathological entities. All lesions showed one of the four types of TDCs in this study. Type A TDC represented those lesions with gradual enhancement without apparent washout, most of the pleomorphic adenomas showed this type. Lev et al[17] reported on the usefulness of the delayed enhancement pattern on contrast-enhanced CT images in differentiating pleomorphic adenomas from malignant parotid tumours. We assume that delayed enhancement on contrast-enhanced CT images corresponds to our Type

Table 2 The average values of CT perfusion parameters for different pathological entities of the parotid gland

Pathological entities	*BV (ml 100 g^{-1})*	*BF (ml 100 g^{-1} min^{-1})*	*MTT (s)*	*PS (ml 100 g^{-1} min^{-1})*
Pleomorphic adenomas	2.8 ± 1.3[a]	44.5 ± 25.1[a]	6.4 ± 3.2	13.0 ± 6.2[a]
Warthin tumours	10.3 ± 4.5[b]	218.5 ± 148.4[b]	4.3 ± 2.1	17.3 ± 8.6
Basal cell adenomas	10.4 ± 3.1[c]	221.2 ± 84.4[c]	3.8 ± 2.6	34.1 ± 9.5[d]
Malignant lesions	5.5 ± 3.0	96.3 ± 59.3	5.4 ± 3.0	24.6 ± 10.3

BF, blood flow; BV, blood volume; MTT, mean transit time; PS, permeability surface.
[a]Differences between pleomorphic adenomas and malignant tumours in BF, BV and PS ($p < 0.05$).
[b]Differences between Warthin tumours and malignant tumours in BF and BV ($p < 0.05$).
[c]Differences between basal cell adenomas and malignant tumours in BF and BV ($p < 0.05$).
[d]Differences in PS between basal cell adenomas and malignant tumours ($p < 0.01$).

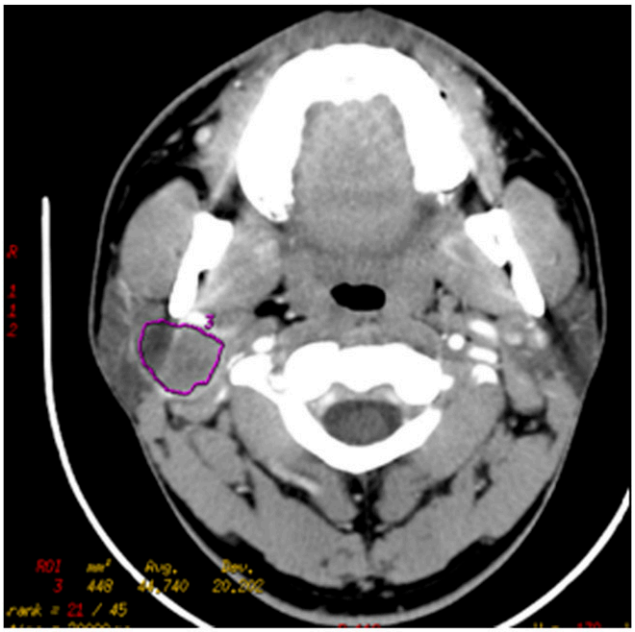

a

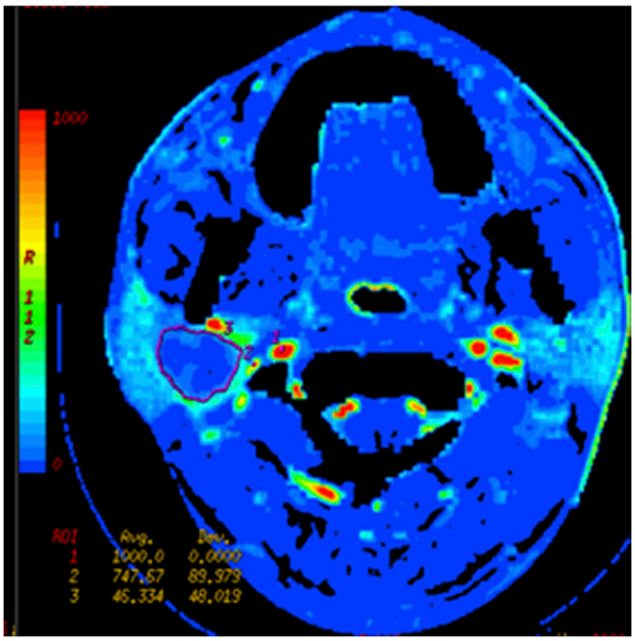

b

Figure 2 A 40-year-old female patient with pleomorphic adenoma in right parotid gland. Late venous source image with hand-drawn region of interest of the tumour (a) and the low level of the BV (b) in the tumour parenchyma.

A TDC pattern. Type B TDC represented those lesions with rapid enhancement and high washout, only all the Warthin tumours showed this type, so the Type B TDC was a specific curve for the diagnosis of Warthin tumours, which was similar to the pattern of early enhancement and fast washout of Warthin tumours in dual-phase CT.[2] Type C TDC represented those with rapid enhancement and medium washout; most of basal cell adenomas and some

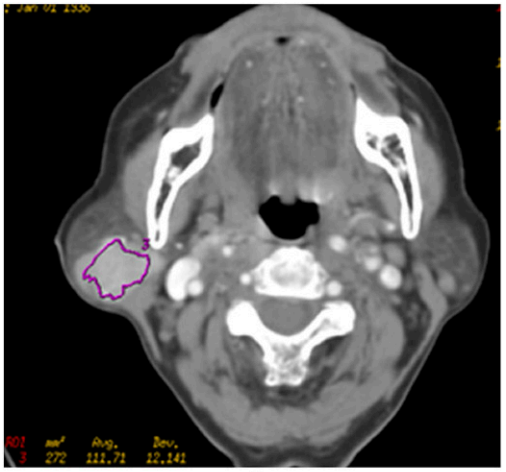

a

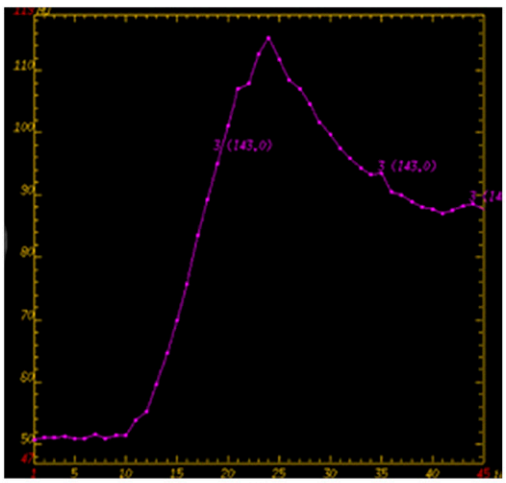

b

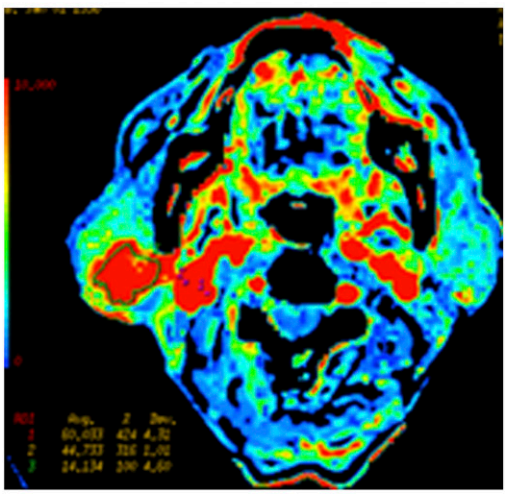

c

Figure 3 A 69-year-old female patient with Warthin tumour in the right parotid gland. Late venous source image with hand-drawn region of interest of the tumour (a), time–density curve (TDC) of the outlined tumour site (b) and blood flow (c). The TDC curve shows a fast enhancement of the neoplasm with a significant continuous washout (about 30 HU) during the remaining acquisition time. Note the high level of blood volume in the tumour parenchyma.

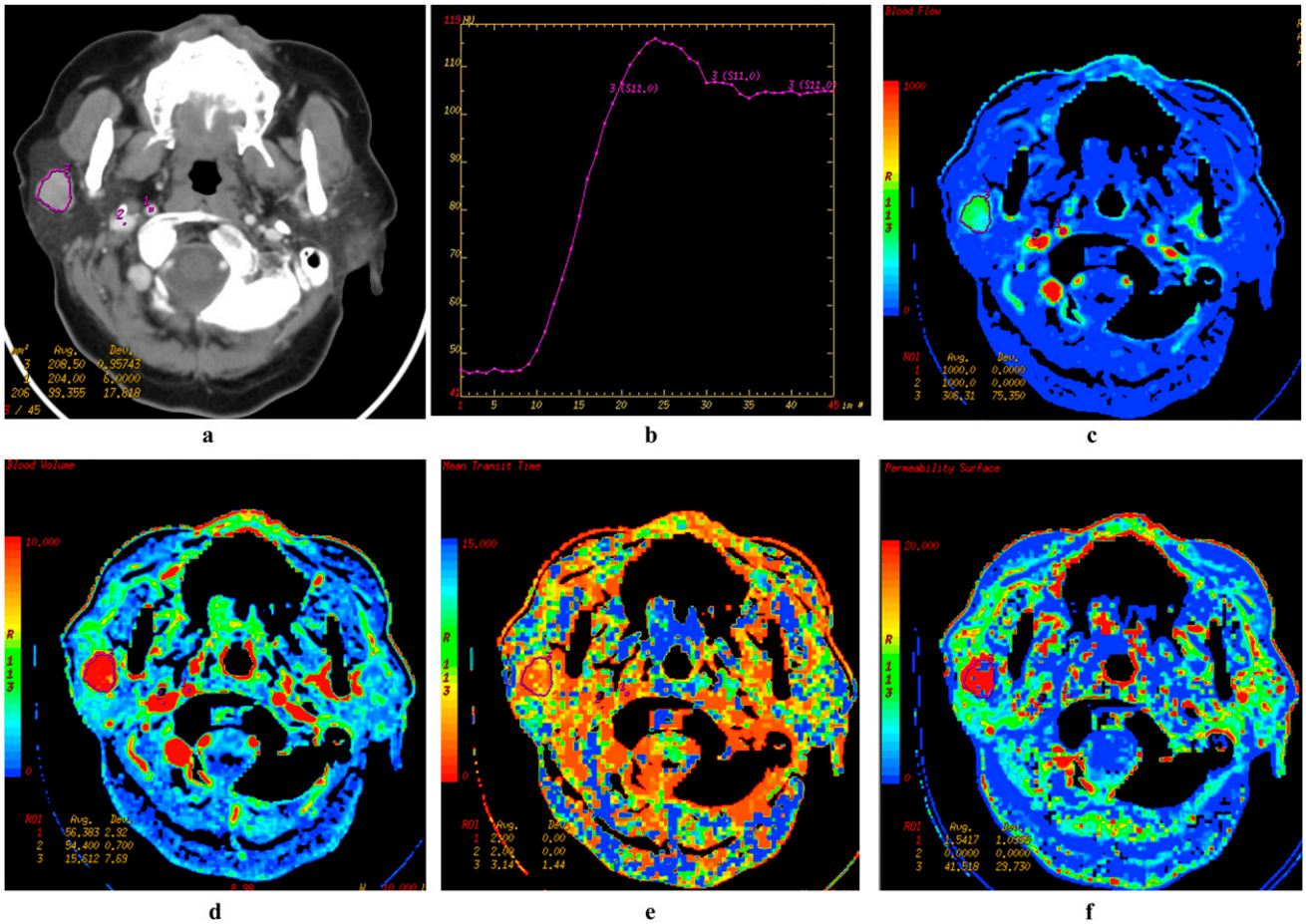

Figure 4 A 72-year-old female patient with basal cell adenoma in the right parotid gland. Late venous source image with hand-drawn region of interest of the tumour (a), time–density curve (TDC) of the outlined tumour site (b), blood flow (BF) (c), blood volume (BV) (d), mean transit time (e), and permeability surface (PS) (f) parametric maps are demonstrated. The TDC also shows an early enhancement of the neoplasm with a light signal drop-off (about 10 HU) and flat during the remaining acquisition time. Note the more elevated BF, BV and PS values (red colour on parametric maps). avg, average; dev, deviation; ROI, region of interest. Colour visible in online version only.

malignant lesions showed this type. Type D TDC represented those with rapid enhancement and low or no washout, most of malignant lesions and three pleomorphic adenomas showed this type. On comparing the TDCs with the corresponding various tumour tissues. Type A TDC was the specific pattern of benign lesion, particularly, for pleomorphic adenomas, which was similar to the pattern of delayed enhancement of the pleomorphic adenomas in dual-phase CT.[2] There were four types of TDC for malignant lesions, and type D was more common. The possible reason was that different kinds of malignant tumours were included in this study, which could be enhanced in different ways.

This study also found the CTP parameters valuable in the differentiation of parotid gland tumours. All previous studies investigated the CTP of the parotid gland by comparing the perfusion parameter differences between malignant and benign tumours. Bisdas et al[12] found that CTP of the parotid gland might differentiate malignant from non-malignant lesions by means of absolute BF, BV and BV ratio values. The measured BF, MTT and PS values of the pleomorphic adenomas and malignant tumours were slightly different from the values reported by Rumboldt et al.[7] But in previous studies, the group of non-malignant lesions included different types of parotid benign tumours. Actually, some benign entities, such as the Warthin tumours and the basal cell adenomas, have ample blood supply, which was different from the hypovascularity of pleomorphic adenomas. This study revealed significantly altered haemodynamic features among the different parotid tumours. There were significantly higher values of BF and BV in Warthin tumours and basal cell adenomas than that of malignant tumours, and, particularly, BF would be >200 ml 100 g^{-1} min^{-1}, as for the other tumours, it was <100 ml 100 g^{-1} min^{-1}. For PS values of basal cell adenomas were higher than that of malignant tumours, whereas that of pleomorphic adenomas was lower than that of malignant tumours. This reflects a faster transmission rate of contrast agent in basal cell adenomas with incomplete and distorted vessel epithelial wall, in consistence with the physiology

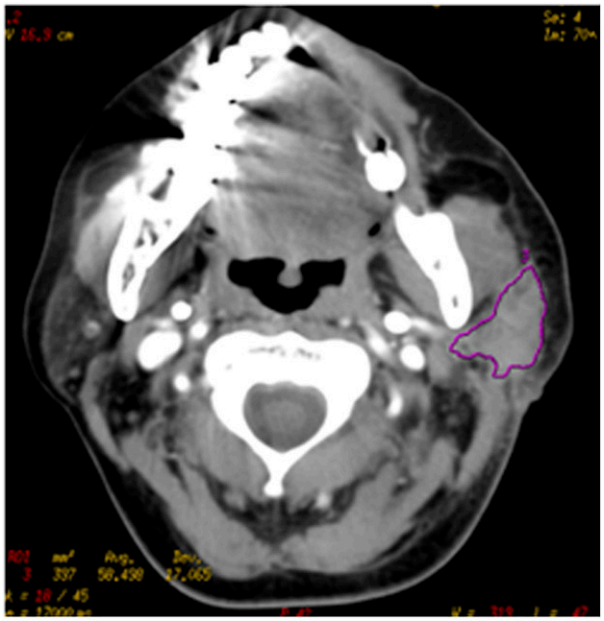

a

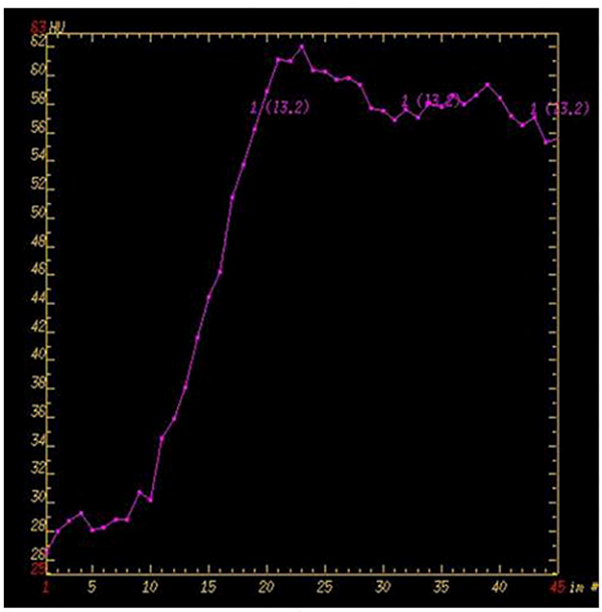

b

Figure 5 A 72-year-old male patient with carcinoma in left parotid gland. Late venous source image with hand-drawn region of interest of the tumour (a), time–density curve (TDC) of the outlined tumour site (b) is demonstrated. The TDC shows also an early enhancement of the neoplasm with a light signal drop-off (about 6 HU) and flat during the remaining acquisition time.

of the neoplastic tissue. Concerning the differentiation of malignant and benign parotid lesions using CTP, if the benign tumour group include various benign entities, it is not appropriate to compare the value of perfusion parameters between benign tumour group and malignant tumour group. The higher BF and BV values of certain benign lesions were apparently anchored to their higher cellularity–stromal grade as compared with the malignant lesions. So, this study focused on the differentiation of different histological categorization of benign tumours from malignant tumours.

In this study, the tables of ROC curves analysis revealed that the perfusion data (BF and BV) had high diagnostic values, which were significantly superior to the MTT and PS in the differentiation of pleomorphic adenomas, Warthin tumours and malignant tumours. The BF, BV and PS have higher diagnostic efficacies than MTT for the differentiation of basal cell adenomas and malignant tumours. Although malignant lesions showed four different types of TDC curve, perfusion data were very useful in the differentiating benign tumours and malignant tumours.

Concerning other modalities besides CT perfusion, some articles reported on the usefulness of diffusion-weighted MR and dynamic enhanced MR in differentiating benign parotid tumours from malignant parotid tumours.[18–21] As Yabuuchi et al[18] previously reported that dynamic enhanced MRI showed high value in the characterization of salivary gland tumours, and time–intensity curve (TIC) patterns suggesting benignancy—Type A (persistent), B (washout) and D (flat) patterns—showed high sensitivity and specificity, whereas the pattern suggesting malignancy—Type C (plateau)—exhibited high sensitivity but relatively low specificity because of the inclusion of some benign tumours. Another research of Yabuuchi et al[19] reported a persistent or flat TIC pattern on dynamic contrast-enhanced MRI indicates benign disease, but there was added value from including the apparent diffusion coefficient (ADC) value in the evaluation of tumours that show a plateau or washout TIC pattern. Dynamic contrast-enhanced MRI need a long scanning time at lest 5 min, so long scanning time, some contraindications and high expense of MRI may also lead to the limited use. So, further studies may be needed to compare CTP imaging with diffusion-weighted and dynamic MRI to establish a priority differentiation method in patients with parotid gland tumours.

Our study has some limitations. First of all, the mean radiation dose of CTP is higher than conventional CT.

Table 3 Receiver operating characteristic (ROC) area, thresholds, sensitivities and specificities for distinguishing pleomorphic adenomas from malignant lesions

Group	*BV*	*BF*	*PS*
ROC area	0.824	0.804	0.690
Thresholds	3.80 ml 100 g^{-1}	55.43 ml 100 g^{-1} min^{-1}	13.79 ml 100 g^{-1} min^{-1}
Sensitivities	75%	75%	71%
Specificities	71%	71%	70%

BV, blood volume; BF, blood flow; PS, permeability surface.

Table 4 Receiver operating characteristic (ROC) area, thresholds, sensitivities and specificities for distinguishing Warthin tumours from malignant lesions

Group	*BV*	*BF*
ROC area	0.809	0.763
Thresholds	7.29 ml 100 g^{-1}	121.94 ml 100 g^{-1} min^{-1}
Sensitivities	0.75%	0.75%
Specificities	0.80%	0.85%

BF, blood flow; BV, blood volume.

Table 5 ROC area, thresholds, sensitivities and specificities for distinguishing basal cell adenomas from malignant lesions

Group	*BV*	*BF*	*PS*
ROC area	0.951	0.902	0.941
Thresholds	8.15 ml 100 g^{-1}	127.09 ml 100 g^{-1} min^{-1}	21.97 s
Sensitivities	0.82%	0.77%	0.94%
Specificities	0.83%	0.83%	0.83%

BF, blood flow; BV, blood volume; PS, permeability surface.

With the second-generation dual energy CT scanners, the radiation dose of CTP is expected to be further reduced with the use of adaptive statistical iterative reconstruction.[22] Secondly, the main limiting factor of the perfusion CT studies was the restricted anatomical coverage currently provided (*i.e.* only 2 cm in the craniocaudal direction with 16-slices scanner). The estimation of the perfusion-associated parameters was restricted to 2.0 cm, which was a known drawback of the CTP imaging as compared with perfusion-weighted MRI,[23] where the gross tumour volume calculation was based on more sections. However, by placing the CTP sections in the region of the largest tumour diameter this pitfall ought to minimize. Also the parotid gland is a surface organ and the neoplasms were found to have diameters <3 cm, so a 2 cm coverage range was enough. Furthermore, the anatomical coverage may be increased to 4 cm for volume perfusion with acquisitions using a 256-slices scanner.[24] In the future, whole tumour data collection will be feasible in clinical applications allowing for a more accurate data analysis. Finally, this investigation reflects our preliminary experience in a small number of patients. Particularly, in the malignant mass group, the limited number of the lesions did not allow research in CTP features of the different types of the malignant masses. Because of the small sample size and overlap in data among the three study subgroups, validation of the proposed cut-off values of CT diagnostic parameters needs to be performed in a large-scale trial.

In conclusion, TDC and perfusion data of CTP imagings show significantly diverse features among the different parotid neoplasms. These results support the use of perfusion CT in the diagnosis and differentiation of parotid neoplasms, although further studies with larger patient population are needed to confirm these findings.

References

1. Lee YY, Wong KT, King AD, Ahuja AT. Imaging of salivary gland tumours. *Eur J Radiol* 2008; **66**: 419–36. doi: 10.1016/j.ejrad.2008.01.027
2. Choi DS, Na DG, Byun HS, Ko YH, Kim CK, Cho JM, et al. Salivary gland tumors: evaluation with two-phase helical CT. *Radiology* 2000; **214**: 231–6. doi: 10.1148/radiology.214.1.r00ja05231
3. Ettl T, Schwarz-Furlan S, Gosau M, Reichert TE. Salivary gland carcinomas. *Oral Maxillofac Surg* 2012; **16**: 267–83. doi: 10.1007/s10006-012-0350-9
4. Schmidt RL, Hall BJ, Wilson AR, Layfield LJ. A systematic review and meta-analysis of the diagnostic accuracy of fine-needle aspiration cytology for parotid gland lesions. *Am J Clin Pathol* 2011; **136**: 45–59.
5. Howlett DC, Kesse KW, Hughes DV, Sallomi DF. The role of imaging in the evaluation of parotid disease. *Clin Radiol* 2002; **57**: 692–701.
6. Jin GQ, Su DK, Xie D, Zhao W, Liu LD, Zhu XN. Distinguishing benign from malignant parotid gland tumours: low-dose multi-phasic CT protocol with 5-minute delay. *Eur Radiol* 2011; **21**: 1692–8. doi: 10.1007/s00330-011-2101-y
7. Rumboldt Z, Al-Okaili R, Deveikis JP. Perfusion CT for head and neck tumors: pilot study. *AJNR Am J Neuroradiol* 2005; **26**: 1178–85.
8. Ng CS, Chandler AG, Wei W, Anderson EF, Herron DH, Charnsangavej C, et al. Reproducibility of perfusion parameters obtained from perfusion CT in lung tumors. *AJR Am J Roentgenol* 2011; **197**: 113–21. doi: 10.2214/AJR.10.5404
9. Petralia G, Fazio N, Bonello L, D'Andrea G, Radice D, Bellomi M. Perfusion computed tomography in patients with hepatocellular carcinoma treated with thalidomide: initial experience. *J Comput Assist Tomogr* 2011; **35**: 195–201. doi: 10.1097/RCT.0b013e31820ccf51
10. Xu J, Liang Z, Hao S, Zhu L, Ashish M, Jin C, et al. Pancreatic adenocarcinoma: dynamic 64-slice helical CT with perfusion imaging. *Abdom Imaging* 2009; **34**: 759–66. doi: 10.1007/s00261-009-9564-1
11. Tawfik AM, Razek AA, Elsorogy LG, Soliman NY, Kerl JM, Mack MG, et al. Perfusion CT of head and neck cancer: effect of arterial input selection. *AJR Am J Roentgenol* 2011; **196**: 1374–80. doi: 10.2214/AJR.10.5343
12. Bisdas S, Baghi M, Wagenblast J, Knecht R, Thng CH, Koh TS, et al. Differentiation of benign and malignant parotid tumors using deconvolution-based perfusion CT imaging: feasibility of the method and initial results. *Eur J Radiol* 2007; **64**: 258–65.
13. Petralia G, Preda L, Raimondi S, D'Andrea G, Summers P, Giugliano G, et al. Intra- and interobserver agreement and impact of arterial input selection in perfusion CT measurements performed in squamous cell carcinoma of the upper aerodigestive tract. *AJNR Am J Neuroradiol* 2009; **30**: 1107–15. doi: 10.3174/ajnr.A1540
14. Miracle AC, Rezaei A, Gandhi D, Mukherji SK. CT perfusion of the neck: internal carotid artery versus external carotid artery as the reference artery. *AJNR Am J Neuroradiol* 2009; **30**: 1598–601. doi: 10.3174/ajnr.A1531
15. Zhang H, Pan Z, Du L, Yan C, Ding B, Song Q, et al. Advanced gastric cancer and perfusion imaging using a multidetector row computed tomography: correlation with prognostic determinants. *Korean J Radiol* 2008; **9**: 119–27. doi: 10.3348/kjr.2008.9.2.119
16. Miles KA, Griffiths MR. Perfusion CT: a worthwhile enhancement? *Br J Radiol* 2003; **76**: 220–31.
17. Lev MH, Khanduja K, Morris PP, Curtin HD. Parotid pleomorphic adenomas: delayed CT enhancement. *AJNR Am J Neuroradiol* 1998; **19**: 1835–9.
18. Yabuuchi H, Matsuo Y, Kamitani T, Setoguchi T, Okafuji T, Soeda H, et al. Parotid gland tumors: can addition of

diffusion-weighted MR imaging to dynamic contrast-enhanced MR imaging improve diagnostic accuracy in characterization? *Radiology* 2008; **249**: 909–16. doi: 10.1148/radiol.2493072045
19. Yabuuchi H, Fukuya T, Tajima T, Hachitanda Y, Tomita K, Koga M. Salivary gland tumors: diagnostic value of gadolinium-enhanced dynamic MR imaging with histopathologic correlation. *Radiology* 2003; **226**: 345–54. doi: 10.1148/radiol.2262011486
20. Eida S, Ohki M, Sumi M, Yamada T, Nakamura T. MR factor analysis: improved technology for the assessment of 2D dynamic structures of benign and malignant salivary gland tumors. *J Magn Reson Imaging* 2008; **27**: 1256–62. doi: 10.1002/jmri.21349
21. Takashima S, Noguchi Y, Okumura T, Aruga H, Kobayashi T. Dynamic MR imaging in the head and neck. *Radiology* 1993; **189**: 813–21. doi: 10.1148/radiology.189.3.8234709
22. Negi N, Yoshikawa T, Ohno Y, Somiya Y, Sekitani T, Sugihara N, et al. Hepatic CT perfusion measurements: a feasibility study for radiation dose reduction using new image reconstruction method. *Eur J Radiol* 2012; **81**: 3048–54. doi: 10.1016/j.ejrad.2012.04.024
23. Eastwood JD, Lev MH, Wintermark M, Fitzek C, Barboriak DP, Delong DM, et al. Correlation of early dynamic CT perfusion imaging with whole-brain MR diffusion and perfusion imaging in acute hemispheric stroke. *AJNR Am J Neuroradiol* 2003; **24**: 1869–75.
24. Kobayashi T, Hayashi T, Funabasama S, Tsukagoshi S, Minami M, Moriyama N. Three-dimensional perfusion imaging of hepatocellular carcinoma using 256-slice multidetector-row computed tomography. *Radiat Med* 2008; **26**: 557–61. doi: 10.1007/s11604-008-0266-3